Defense of Bachelor Thesis

Mapping Study of 71 *Planck* Cold Clumps in Taurus/Perseus/California Complexes

FANYI MENG

Supervisor: Prof. YUEFANG WU

PEKING UNIVERSITY

June 7, 2013

Outline

- Introduction
- Observation
- Results and Analysis
  - Gas Emission
  - Physical Parameters
  - Turbulence
  - Gas-Dust Coupling
  - Stability of Cores
  - Associated Objects
- Summary

1 Introduction

- *Planck* space telescope, working at mm/sub-mm bands, systematically investigated galactic cold dust cores and presented *Planck*Early Release Cold Cores Catalog (ECC).
- ECC contains 915 most reliable (SNR > 15 and $T_{\rm ECC} < 14$ K) detections (Planck Collaboration 2011).
- Besides the dust observation made by Planck Collaboration, study of gas components of these cores is of urgent necessity.
- Millimeter line follow-up studies of Planck Cold Cores were conducted by our group:
  - A single point survey toward 674 *Planck*Cold Clumps of ECC in the $J = 1 - 0$ transitions of ^{12}CO , ^{13}CO , and C^{18}O has been carried out using the Purple Mountain Observatory 13.7 m Telescope.

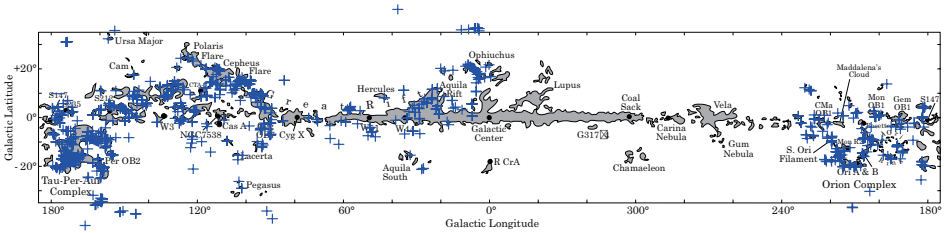

Figure 1: The *Planck* Cold Clumps studied by Wu et al. (2012) are plotted as +, over Milky Way regions map by Dame et al. (2001).

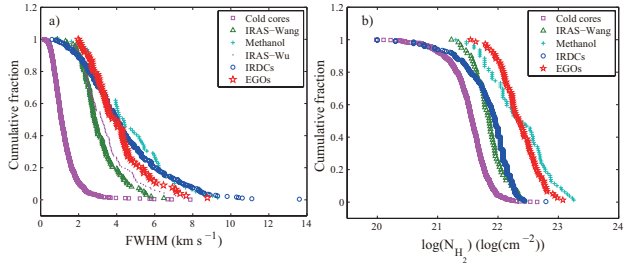

Figure 2: We compare the line widths of ^{13}CO$(1-0)$ and column densities with the CO molecular line surveys toward different kind of targets.

- Besides our single point study, we have conducted the mapping survey of the 71 Planck Cold Cores in Taurus Molecular Cloud (TMC), Perseus Molecular Cloud (PMC) and California Molecular Cloud (CMC).

- TMC contains ideal samples for studying characteristics of early stage in star formation. Outflows (Wu et al. 2004), T Tau binary system (van Langevelde et al. 1994) , disks around HL Tau young stars (Sargent and Beckwith 1991), DM Tau (Saito et al. 1995) were all found in it. TMC contains class 0-III sources.

- PMC: intermediate mass star forming region (Lombardi et al. 2010). Star formation in PMC is between the low-mass (in TMC) and high-mass (in Orion) star formation (Johnstone et al. 2010).

- CMC is rarely studied before Lada et al. (2009). CMC is revealed similar to Orion in distance, mass and morphology, but with much lower star forming activity (Lada et al. 2009,Lombardi et al. 2010).

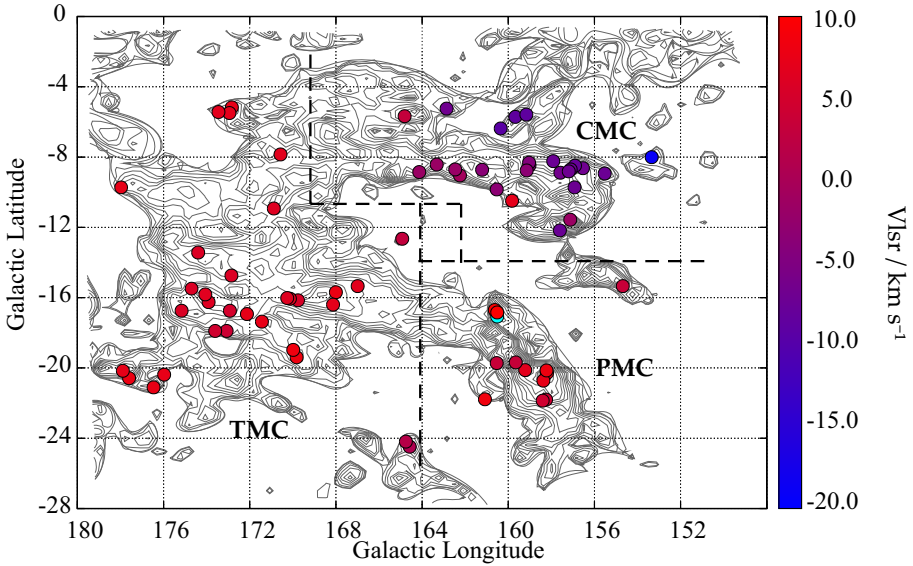

Figure 3: The 71 sources we mapped. Contours: CO integrated intensity map by Dame et al. (2001).

2 Observation

The $J = 1 \rightarrow 0$ ^{12}CO , ^{13}CO and C^{18}O lines were observed using 13.7 m telescope of Qinghai Station of Purple Mountain Observatory, from January to May, 2011.

Condition of Observation

Half-power beam size	$56'' \times 55''$(at 92.8GHz)
Main beam efficiency	$\sim$50%
Pointing accuracy	better than $4''$
Spectral resolution	for ^{12}CO$(1-0)$: 0.16 km s^{-1}
	for ^{13}CO$(1-0)$, C^{18}O$(1-0)$: 0.17 km s^{-1}
T_A^* rms noise	for ^{12}CO$(1-0)$: 0.2 K
	for ^{13}CO$(1-0)$, C^{18}O$(1-0)$: 0.1 K
OTF scan speed	$20''$s^{-1}

Figure 4: Picture of PMO 13.7 m Telescope, from CAS website.

3 Results and Analysis

3.1 Gas Emission

- $^{12}CO(1-0)$ and $^{13}CO(1-0)$ emissions detected: all the 71 clumps
- $C^{18}O(1-0)$ emissions detected: 55 clumps

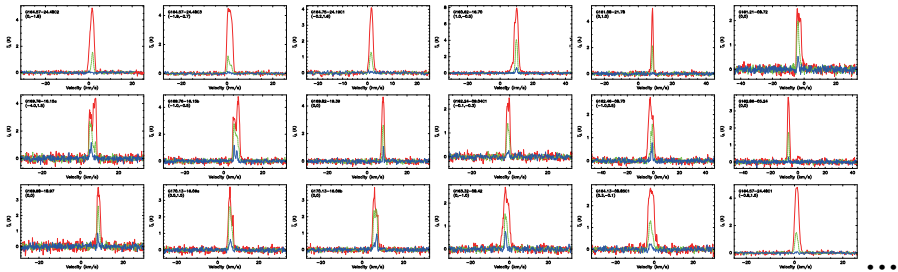

Figure 5: Examples of $^{12}CO(1-0)$ (red), $^{13}CO(1-0)$ (green) and $C^{18}O(1-0)$ (blue) spectra detected at intensity peaks.

Gaussian fitting was adopted for all three lines, and observed line parameters were obtained for each spectra, at peaks of integrated intensity.

Table 1: Observed line parameters (16 rows of the totally 82 rows)

Source	v_{lsr}(12) (km/s)	FWHM (12) (km/s)	Ta (12) (K)	v_{lsr}(13) (km/s)	FWHM(13) (km/s)	Ta(13) (K)	v_{lsr} (18) (km/s)	FWHM (18) (km/s)	Ta (18) (K)	
G154.68-15.34C1	3.37(0.07)	1.61(0.19)	4.09(0.74)	3.34(0.01)	0.96(0.03)	2.59(0.1)				
G156.92-09.72C1	-7.36(0.02)	2.23(0.05)	2.54(0.15)	-7.24(0.01)	1.39(0.03)	1.54(0.05)	-7.36(0.07)	1.12(0.28)	0.29(0.06)	BA
G157.12-11.56C1	-1.98(0.02)	1.96(0.04)	4.44(0.21)	-1.68(0.01)	1.23(0.02)	2.43(0.07)	-1.63(0.03)	0.87(0.06)	0.55(0.07)	
G157.12-11.56C2	-1.94(0.02)	2.05(0.05)	4.3(0.23)	-1.7(0.01)	1.28(0.03)	2.03(0.07)	-1.66(0.06)	0.88(0.12)	0.36(0.08)	
G157.12-11.56C3	-1.79(0.02)	2.19(0.06)	4.58(0.26)	-1.72(0.02)	1.14(0.05)	1.93(0.13)				W
G157.60-12.17bC1	-2.89(0.01)	2.53(0.02)	5.44(0.09)	-2.57(0.01)	1.15(0.03)	2.68(0.59)	-2.4(0.07)	0.71(0.14)	0.24(0.07)	
G157.60-12.17bC2	-2.44(0.02)	2.89(0.04)	5.11(0.18)	-1.97(0.03)	1.82(0.09)	1.69(0.11)				
G157.91-08.23C1	-7.28(0.02)	3.25(0.05)	2.38(0.11)	-7.31(0.01)	2.05(0.03)	1.92(0.07)	-7.49(0.05)	1.4(0.1)	0.53(0.08)	
G159.21-20.12C1	6.41(0.01)	4.44(0.01)	5.75(0.07)	6.63(0.01)	2.14(0.01)	4.88(0.06)	6.69(0.01)	1.2(0.03)	1.87(0.06)	
G160.51-17.07	10.41 (0.01)	2.82 (0.03)	5.92 (0.14)	10.43 (0.01)	1.57 (0.02)	3.46 (0.09)	10.6 (0.06)	1.13 (0.13)	0.49 (0.09)	
G160.53-09.84	-3.29 (0.01)	2.01 (0.01)	5.56 (0.09)	-3.51 (0.01)	1.44 (0.01)	2.88 (0.06)	-3.66 (0.03)	0.88 (0.09)	0.53 (0.07)	
G160.62-16.70	9.9 (0.01)	2.7 (0.02)	7.93 (0.17)	9.98 (0.01)	1.41 (0.01)	4.24 (0.07)	10.01 (0.04)	1.1 (0.08)	0.63 (0.07)	
G161.21-08.72	-3.27 (0.02)	3.04 (0.05)	2.42 (0.11)	-3.87 (0.02)	1.56 (0.04)	2 (0.09)	-3.78 (0.05)	0.91 (0.1)	0.51 (0.09)	
G163.32-08.42	-1.64 (0.02)	3.3 (0.04)	2.51 (0.09)	-1.78 (0.02)	1.64 (0.04)	1.48 (0.08)	-1.94 (0.03)	0.91 (0.06)	0.77 (0.08)	
G168.00-15.69	7.82 (0.03)	1.67 (0.07)	4.86 (0.37)	7.71 (0)	0.97 (0.01)	3.56 (0.06)	7.67 (0.01)	0.57 (0.02)	1.29 (0.07)	
G168.13-16.39	6.07 (0.03)	1.18 (0.06)	3.91 (0.14)	6.99 (0.02)	0.84 (0.05)	2.79 (0.08)	6.37 (0.02)	0.42 (0.06)	1.27 (0.1)	

• • •

3.2 Physical Parameters

From the Gaussian fitting results, physical parameters such as excitation temperature ($T_{\rm ex}$), column density of H_2 ($N_{\rm H_2}$), velocity dispersions (σ_{Therm} , σ_{NT} and σ_{3D}) for each core and clump were derived.

$$T_{ex} = T_0 / \ln[T_0 (T_R^* + T_0 \exp{(-T_0/T_{bg})} - 1)]$$

$$N_{tot} = \frac{3k}{8\pi^3 B \mu^2} \frac{\exp[hBJ(J+1)/kT_{ex}]}{(J+1)} \frac{(T_{ex} + hb/3k)}{[1 - \exp(-h\nu/kT_{ex})]} \int \tau_v \, dv \text{ (Garden et al. 1991)}$$

$$\sigma_{Therm} = \left(\frac{kT_{ex}}{m_H \mu} \right)^{1/2}, \sigma_{NT} = \left(\sigma^2_{^{13}\rm CO} - \frac{kT_{ex}}{m_{^{13}\rm CO}} \right)^{1/2} \text{ and } \sigma_{3D} = \sqrt{3(\sigma^2_{Therm} + \sigma^2_{NT})}$$

For them who have $C^{18}O(1-0)$ detections.

$$\sigma_{NT} = \left(\sigma^2_{\rm C^{18}O} - \frac{kT_{ex}}{m_{\rm C^{18}O}} \right)^{1/2}$$

Employing the same methods, we calculated these parameters for every pixels ($0.5' \times 0.5'$) of each map.

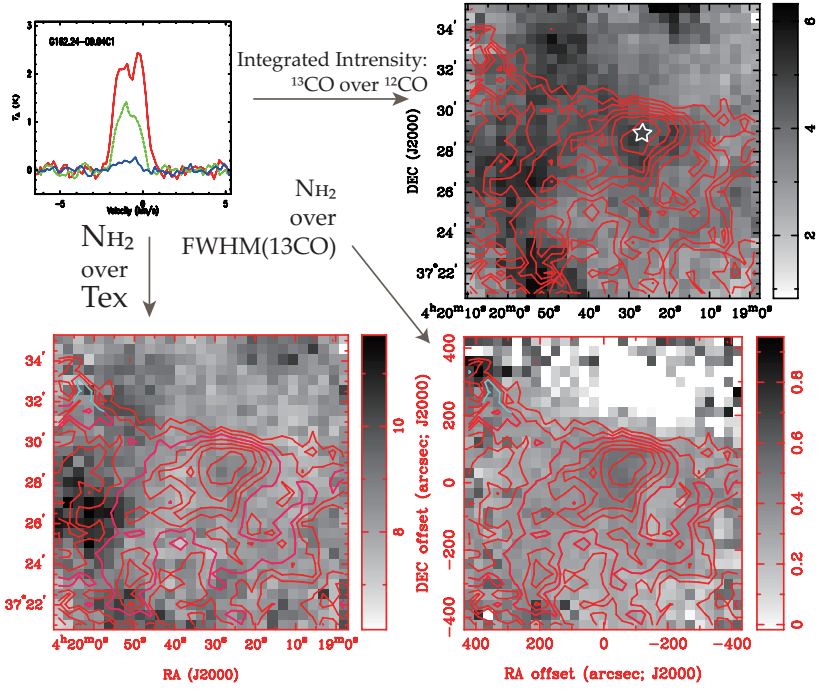
Integrated Intrensity:
13CO over 12CO
NH2
over
FWHM(13CO)
NH2
over
Tex
DEC (J2000)
RA (J2000)
DEC offset (arcsec; J2000)
RA offset (arcsec; J2000)

Average value of physical parameters over mapping area within 50% peak intensity isolines for 38 cores were calculated.

Table 2: Physical parameters of cores(20 of 38 rows)

Name	V_{lsr}	Offset	Deconvolved Size	R	T_{ex}	N_{H_2}	σ_{Therm}	σ_{NT}	σ_{3D}	n	M_{LTE}	M_{vir}	M_J	Region
	$km\,s^{-1}$	($''$,$''$)	($''\times''(^\circ)$)	(pc)	(K)	(10^{21} cm^{-2})	($km\,s^{-1}$)	($km\,s^{-1}$)	($km\,s^{-1}$)	($\frac{10^3}{cm^{-3}}$)	($M_\odot$)	($M_\odot$)	($M_\odot$)	
G153.34-08.00C1	-18.93	(6 , -49)	196 × 107 (-13.2)	0.158	9.7 (0.5)	2.0 (0.7)	0.19(0.005)	0.34(0.04)	0.66(0.07)	2.0	2.9	43	19	CMC
G153.34-08.00C2	-19.10	(-163, 120)	224 × 86 (-21.0)	0.151	10.3(0.4)	1.5 (0.4)	0.19(0.003)	0.30(0.05)	0.60(0.07)	1.6	2.0	35	17	CMC
G154.68-15.34C1	3.31	(216 ,31)	1261× 381 (72.4)	0.394	11.9(0.9)	2.2 (0.7)	0.21(0.008)	0.32(0.09)	0.65(0.14)	0.9	20	76	28	PMC
G155.52-08.93C1	-7.46	(18 ,-2)	392 × 284 (-13.8)	0.364	9.7 (1.0)	1.0 (0.3)	0.18(0.009)	0.22(0.05)	0.48(0.07)	0.5	7.8	49	15	CMC
G156.92-09.72C1	-7.19	(50 , 53)	714 × 421 (-12.7)	0.598	9.0 (0.4)	1.8 (0.4)	0.18(0.004)	0.33(0.08)	0.64(0.13)	0.5	38	160	35	CMC
G157.12-11.56C1	-1.79	(-12 , 84)	383 × 238 (-55.4)	0.331	6.3 (0.9)	3.0 (0.7)	0.15(0.010)	0.26(0.05)	0.51(0.08)	1.5	19	53	10	CMC
G157.12-11.56C2	-1.90	(-50 , 137)	694 × 269 (-4.7)	0.473	6.2 (0.7)	2.7 (0.9)	0.15(0.009)	0.26(0.06)	0.52(0.09)	0.9	35	77	13	CMC
G157.12-11.56C3	-1.62	(-38 , -352)	173 × 102 (75.9)	0.145	5.3 (0.2)	2.4 (0.8)	0.14(0.003)	0.45(0.08)	0.81(0.13)	2.8	3.0	40	30	CMC
G157.60-12.17C1	-7.68	(67 , -45)	405 × 335 (-23.6)	0.402	10.5(1.0)	2.4 (0.8)	0.19(0.009)	0.28(0.09)	0.59(0.13)	0.9	23	76	20	CMC
G157.60-12.17bC1	-2.55	(-92 , -59)	513 × 372 (39.7)	0.476	14.9(1.5)	3.0 (0.9)	0.23(0.012)	0.21(0.10)	0.54(0.15)	1.0	40	50	14	CMC
G157.60-12.17bC2	-2.32	(-187, -266)	281 × 213 (61.4)	0.267	14.7(1.3)	2.9 (0.9)	0.23(0.010)	0.61(0.14)	1.11(0.23)	1.8	12	190	98	CMC
G157.91-08.23C1	-7.23	(31 , -106)	524 × 494 (31.6)	0.556	8.5 (0.6)	2.8 (0.8)	0.17(0.005)	0.41(0.13)	0.77(0.21)	0.8	51	230	47	CMC
G159.21-20.12C1	6.53	(47 , 3)	877 × 633 (-32.5)	0.425	16.1(1.3)	10.7(2.6)	0.24(0.010)	0.35(0.13)	0.74(0.21)	4.1	110	130	18	PMC
G159.67-05.71C1	-8.50	(-17 , -12)	469 × 418 (-9.4)	0.482	9.4 (0.6)	2.0 (0.9)	0.18(0.006)	0.51(0.13)	0.94(0.20)	0.7	27	410	90	CMC
G159.82-10.48C1	7.00	(23 , -7)	453 × 263 (-24.1)	0.376	12.4(0.7)	2.1 (0.7)	0.21(0.006)	0.41(0.09)	0.79(0.14)	0.9	17	150	49	CMC
G160.35-06.37C1	-9.2	(8 , -47)	238 × 79 (43.3)	0.149	8.6 (0.7)	1.3 (0.5)	0.17(0.008)	0.27(0.08)	0.55(0.11)	1.6	1.7	33	12	CMC
G160.53-19.72C1	3.56	(6 , 89)	864 × 473 (-62.6)	0.364	12.8(0.7)	4.2 (1.3)	0.21(0.005)	0.34(0.11)	0.71(0.18)	1.8	33	100	23	PMC
G162.24-09.04C1	-0.82	(-5 , -19)	562 × 377 (-78.6)	0.501	8.3 (0.4)	1.6 (0.5)	0.17(0.004)	0.37(0.08)	0.70(0.13)	0.5	23	230	45	CMC
G164.13-08.85C1	-1.66	(19 , -6)	709 × 372 (35.2)	0.559	9.9 (0.8)	2.3 (0.7)	0.19(0.008)	0.41(0.11)	0.78(0.17)	0.7	42	230	52	CMC
G164.57-24.48C1	0.90	(-49 , 90)	226 × 90 (-59.5)	0.048	12.6(0.6)	1.7 (0.5)	0.22(0.005)	0.35(0.07)	0.69(0.11)	5.6	0.23	19	14	TMC

• • •

From all the 71 clumps, we got the integrated intensity map for both $^{12}CO(1-0)$ and $^{13}CO(1-0)$, Shown as red contours (^{12}CO) over greyscale background (^{13}CO).

Right shows one page of all the 5 pages of maps.

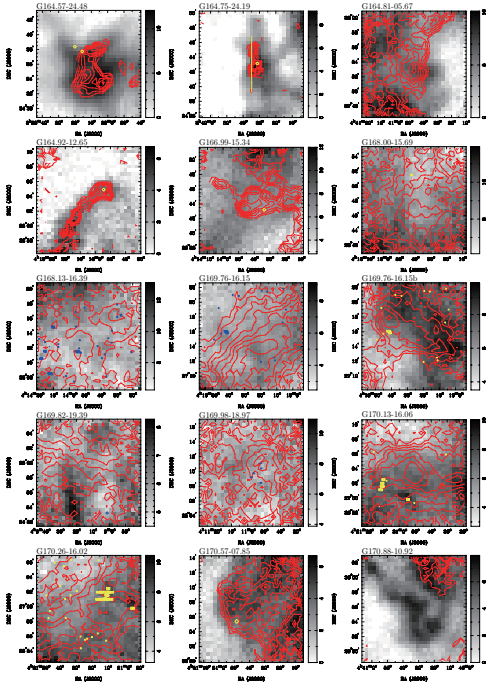

3.3 Turbulence dominated cores

Most of the cores (in both TMC and CMC) are found with $\sigma_{NT} > \sigma_{Therm}$, indicating the dominance of turbulence.

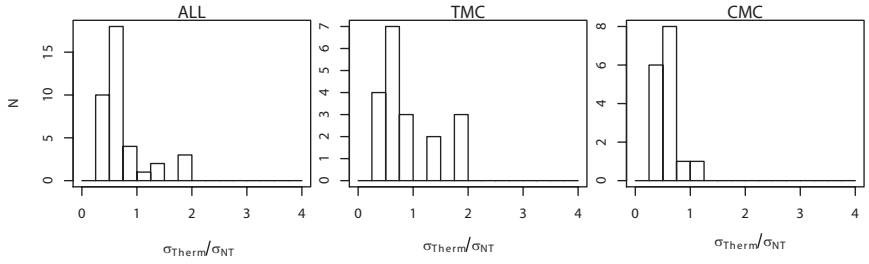

The dominance of turbulence indicates that the gravitational contracting/collapse is rare in our cores of both regions, otherwise the turbulence will soon decay on a dynamic timescale (Shu et al. 1987).

We tested the probability distribution function (PDF) of $N_{\rm H_2}$ in our cores, and good ($p > 0.05$ in K-S test) log-normal distribution were found, without exhibiting "power-law tail". Such log-normal PDFs indicate that turbulence is dominating the density structure of gas in our cores. We compare our results with the gravity affected PDF by Schneider et al. (2013).

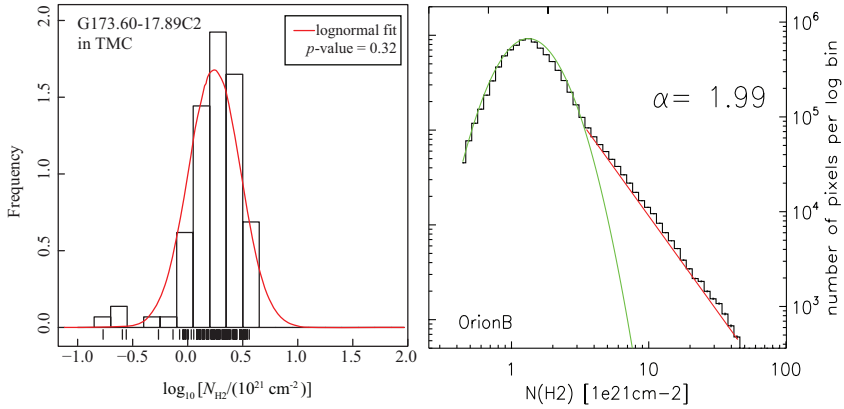

We tested the probability distribution function (PDF) of $N_{\mathrm{H_2}}$ in our cores, and good ($p > 0.05$ in K-S test) log-normal distribution were found, without exhibiting "power-law tail". Such log-normal PDFs indicate that turbulence is dominating the density structure of gas in our cores. We compare our results with the gravity affected PDF by Schneider et al. (2013).

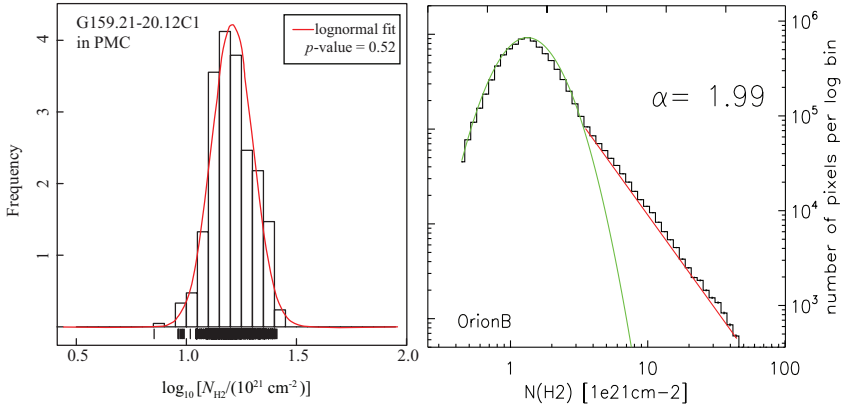

We tested the probability distribution function (PDF) of $N_{\rm H_2}$ in our cores, and good ($p > 0.05$ in K-S test) log-normal distribution were found, without exhibiting "power-law tail". Such log-normal PDFs indicate that turbulence is dominating the density structure of gas in our cores. We compare our results with the gravity affected PDF by Schneider et al. (2013).

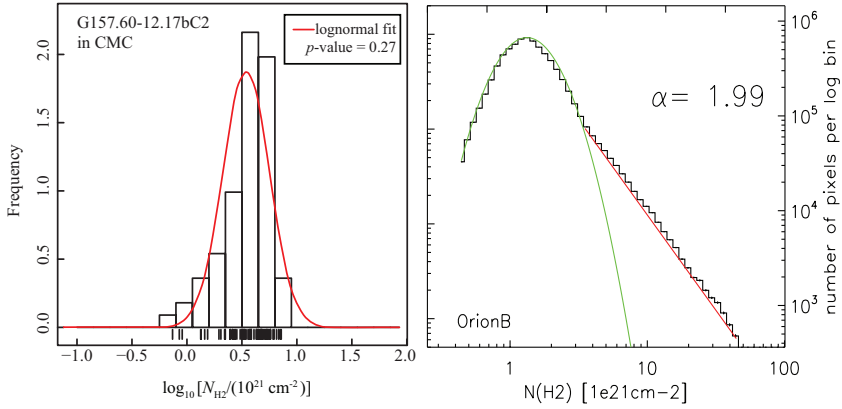

3.4 Stability of Cores

Most of the cores are found with LTE mass less than Jeans Mass and virial mass, indicating that these cores are generally stable.

TMC:

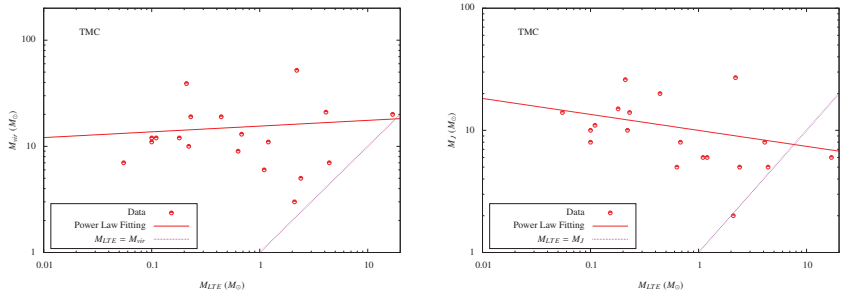

Left panel: The correlation between M_{LTE} and M_{vir}. Right panel: The correlation between M_{LTE} and M_J. The red line is the power law fitting function, while the blue dotted line is the $M_{LTE} = M_{vir}$line, which also is the critical line for gravitational bound state (below the line).

CMC:

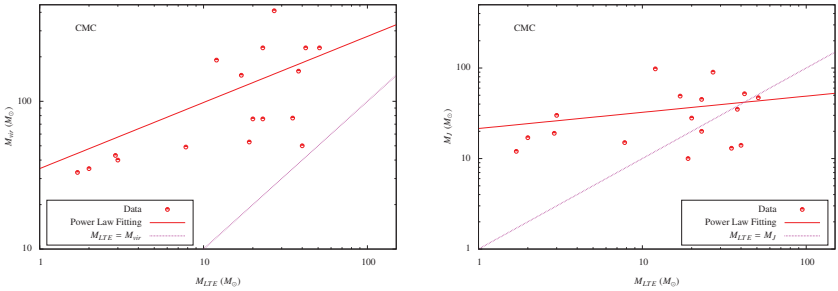

Left panel: The correlation between M_{LTE} and M_{vir}. Right panel: The correlation between M_{LTE} and M_J. The red line is the power law fitting function, while the blue dotted line is the $M_{LTE} = M_{vir}$line, which also is the critical line for gravitational bound state (below the line).

3.5 Coupling of Gas and Dust

3.5.1 Temperature

Majority of the cores are found with $T_D > T_K$, consisting with the Goldreich-Kwan picture (Goldreich and Kwan, 1974).

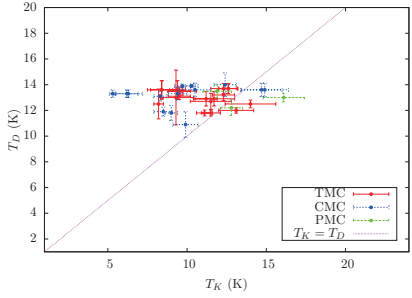

Figure 6: Correlation of Gas-Dust temperature

3.5.2 Column Density

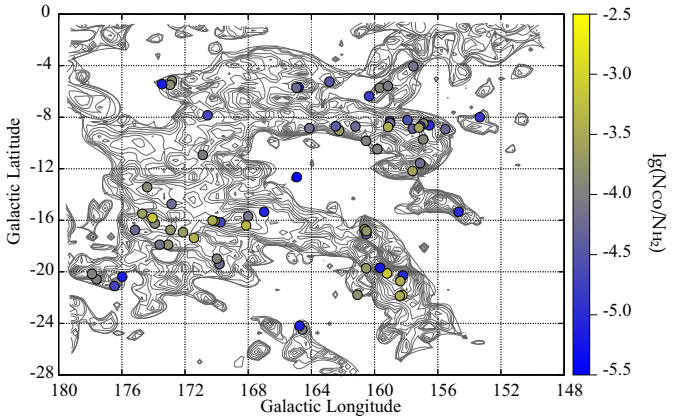

Figure 7: CO abundance calculated from CO emission ($N_{^{12}CO}$) and Planck ECC data (N_{H_2}); Background: The contours of ^{13}CO data from (Dame et al., 2001)

3.6 Associated Objects

Most of the cores are without associated objects in the confine of circle of radius as same as beam size ($\sim$ 1 arc min) at there centers. The few exceptions are the cores that are:

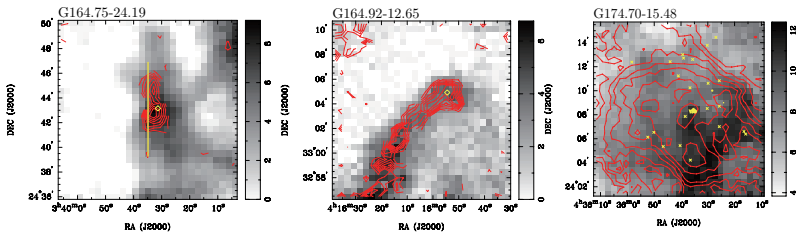

Thus, despite that 70 % of the cores are found with associated objects mentioned above, 34 of 38 cores are without associated objects within their center parts, suggesting that they are sourceless. Remarkably, for the three cores with associated sources in TMC: G164.75-24.19C2 and G164.92-12.65C1 are both with σ_{Therm} larger than σ_{NT} . G174.70-15.48C1 is with $T_{\rm ex}$ of 14.0 K, which is the highest among the cores in TMC, also indication a later revolutionary stage.

4 Summary

71 Planck cold clumps in TMC, CMC and PMC were mapped with ^{12}CO$(1-0)$, ^{13}CO$(1-0)$ and C^{18}O$(1-0)$, respectively. Physical parameters such as $T_{\rm ex}$, $N_{\rm H_2}$, σ_{Therm} , σ_{NT} , σ_{3D} were calculated for each of the clumps and the cores within them. By analyzing these physical parameters, several significant questions could be responded:

- What role turbulence plays in Planck cold clumps?
  - Turbulence dominates the broadening of spectra, revealing Planck cores are generally inmature.
- Are these clumps stable or have cores inside that will gravitationally collapse?
  - Majority of the cores are revealed stable in our research. But further study with higher resolution is still needed to warrant or deny it.
- How the gas and dust coupled?
  - Gas are slightly colder than dust in core region. CO abundance is higher in the center of complexes

- Are these cores sourceless or not?
  - Most of the cores are sourceless. For the cores associated with source, they show hints of collapsing.

These results suggest that Planck Cold Clumps are fairly excellent examples for studying the formation of stars and even the formation of molecular clouds. The paper has been submitted to *ApJS* and has past second review by the referee.

Thanks!

References

Dame, T. M., Hartmann, D., and Thaddeus, P.: 2001, *ApJ* **547**, 792

Goldreich, P. and Kwan, J.: 1974, *ApJ* **189**, 441

Johnstone, D., Rosolowsky, E., Tafalla, M., and Kirk, H.: 2010, *ApJ* **711**, 655

Lada, C. J., Lombardi, M., and Alves, J. F.: 2009, *ApJ* **703**, 52

Lombardi, M., Lada, C. J., and Alves, J.: 2010, *A&A* **512**, A67

Planck Collaboration: 2011, *A&A* **536**, A22

Saito, M., Kawabe, R., Ishiguro, M., Miyama, S. M., Hayashi, M., Handa, T., Kitamura, Y., and Omodaka, T.: 1995, *ApJ* **453**, 384

Sargent, A. I. and Beckwith, S. V. W.: 1991, *ApJL* **382**, L31

Schneider, N., André, P., Könyves, V., Bontemps, S., Motte, F., Federrath, C., Ward-Thompson, D., Arzoumanian, D., Benedettini, M., Bressert, E., Didelon, P., Di Francesco, J., Griffin, M., Hennemann, M., Hill, T., Palmeirim, P., Pezzuto, S., Peretto, N., Roy, A., Rygl, K. L. J., Spinoglio, L., and White, G.: 2013, *ApJL* **766**, L17

Shu, F., Adams, F., and Lizano, S.: 1987, *ARA&A* **25**, 23

van Langevelde, H. J., van Dishoeck, E. F., and Blake, G. A.: 1994, *ApJL* **425**, L45

Wu, Y., Liu, T., Meng, F., Li, D., Qin, S.-L., and Ju, B.-G.: 2012, *ApJ* **756**, 76

Wu, Y., Wei, Y., Zhao, M., Shi, Y., Yu, W., Qin, S., and Huang, M.: 2004, *A&A* **426**, 503